Simulation of Multifrequency EPR Spectra from Mn(III)/Mn(IV) Catalase of *Lactobacillus plantarum* Using a New Approach Based on Perturbation Theory

Alice Haddy,*,†,[1a,c] Geoffrey S. Waldo,‡,[1b] Richard H. Sands,[1a] and James E. Penner-Hahn*,[1b]

Biophysics Research Division and Department of Chemistry, University of Michigan, Ann Arbor, Michigan 48109, and Section of Hematology Research, Mayo Clinic and Foundation, Rochester, Minnesota 55905

Received November 4, 1993®

The 16-line EPR signal from the Mn(III)/Mn(IV) state of *Lactobacillus plantarum* Mn catalase was studied at three microwave frequencies: S-band (3.0 GHz), X-band (9.2 GHz), and P-band (15.5 GHz). The spectra were simulated using a program that calculated the hyperfine splitting as a perturbation of the Zeeman term to third order. The transition energies were calculated numerically from the perturbation terms rather than from an explicit expression derived from perturbation theory, as has been done previously for spectra from multinuclear Mn complexes. Nine Mn catalase spectra were fit using a nonlinear least-squares minimization routine assuming an axial $S = {}^1/_2$ system. Axial **g** and hyperfine matrices were found to fit the spectra well. Second-order perturbation theory was sufficient to fit the X- and P-band spectra, but third-order perturbation terms were necessary to adequately fit the S-band spectrum and give parameters that agreed with those found at the higher frequencies. The EPR parameters found for this biological Mn dimer ($g_z = 1.990$, $g_x = g_y = 2.008$, $A_{1z} = 104.1 \times 10^{-4}$ cm^{-1}, $A_{1x} = A_{1y} = 141.6 \times 10^{-4}$ cm^{-1}, $A_{2z} = 83.5 \times 10^{-4}$ cm^{-1}, $A_{2x} = A_{2y} = 76.0 \times 10^{-4}$ cm^{-1}) compare well with those for synthetic Mn(III)/Mn(IV) complexes and with estimates by vector projection using literature values of the independent Mn ions. The success of the simulation method employed here, which can accommodate rhombic systems and carry the perturbation calculation to third or higher orders, will have utility for simulation of the S_2 multiline signal at $g = 2$ from the O_2-evolving complex of higher plants and algae.

Introduction

The catalase enzyme catalyzes the disproportionation of H_2O_2 into H_2O and O_2. The catalases from *Lactobacillus plantarum*, *Thermus thermophilus*, and *Thermoleophilum album*[2-5] contain a dinuclear Mn cluster at the active site.[6-11] A 16-line EPR signal characteristic of a coupled Mn(III)/Mn(IV) cluster in the $S = {}^1/_2$ ground state has been observed for both the *L. plantarum* and *T. thermophilus* catalases.[6-9] Analysis of the XANES spectra for the *L. plantarum* catalase have confirmed the assignment of Mn(III)/Mn(IV) as the valence state giving rise to this signal.[11]

The Mn catalase multiline signal is of special interest because of its similarity to the multiline signal at $g = 2$ from the S_2 oxidation state of the O_2-evolving complex (OEC) of higher plants.[12-15] In the OEC, the $g = 2$ multiline signal is believed to come from a trimer or tetramer of Mn(III) and/or Mn(IV). Like the OEC, the metal center of Mn catalase can take on several oxidation states.[6-9,11,16] EPR signals attributed to the even-spin Mn(II)/Mn(II) state have been observed, and a third EPR-visible form, assigned to a Mn(II)/Mn(III) mixed-valence species, is also known.[6-8] The enzyme is active in its reduced form and apparently cycles between the Mn(II)/Mn(II) and Mn(III)/Mn(III) states.[10,11] The Mn(III)/Mn(IV) form, which is the subject of the present communication, is catalytically inactive.[7,11]

We report here a detailed EPR analysis of the Mn(III)/Mn(IV) form of the *L. plantarum* Mn catalase, which reveals features relevant to the chemical nature of the Mn dimer. The spectral simulation method employed calculates hyperfine shifts by perturbation theory to third order on the basis of a direct numerical approach. The method allows accurate calculation of isotropic, axial, or rhombic spectra from a variety of microwave frequencies and therefore can provide an unambiguous interpretation of an EPR signal. The EPR parameters found here for the Mn catalase signal at the three frequencies employed agree with one another as well as with previous studies of Mn catalase spectra,[13,17] confirming the utility of this simulation method for low as well as conventional X-band frequencies. The simulation method can potentially provide spectroscopic insight into the more complex multiline EPR signal from the photosynthetic O_2-evolving cluster of higher plants and algae.

Experimental Section

Mn catalase was isolated from *L. plantarum* as previously described[11] and stored at 80 K in 50 mM sodium phosphate, pH 7.0, and 0.1 mM EDTA (buffer A). The concentration of enzyme for EPR experiments

* Authors to whom correspondence should be addressed.
† Present address: Section of Hematology Research, Mayo Clinic and Foundation, Rochester, MN 55905.
‡ Present address: Department of Biochemistry, North Carolina State University, Raleigh, NC 27695.
® Abstract published in *Advance ACS Abstracts*, May 15, 1994.

(1) (a) Biophysics Research Division, University of Michigan. (b) Department of Chemistry, University of Michigan. (c) Mayo Clinic.
(2) Kono, Y.; Fridovich, I. *J. Biol. Chem.* **1983**, *258*, 6015.
(3) Beyer, W. F., Jr.; Fridovich, I. *Biochemistry* **1985**, *24*, 6460.
(4) Barynin, V. V.; Grebenko, A. I. *Dokl. Akad. Nauk. SSSR* **1986**, *286*, 461.
(5) Allgood, G. S.; Perry, J. J. *J. Bacteriol.* **1986**, *168*, 563.
(6) Barynin, V. V.; Vagin, A. A.; Melik-Adamyan, V. R.; Grebenko, A. I.; Khangulov, S. V.; Popov, A. N.; Andrianova, M. E.; Vainshtein, B. K. *Sov. Phys.—Dokl. (Engl. Transl.)* **1986**, *31*, 457.
(7) Khangulov, S. V.; Barynin, V. V.; Antonyuk-Barynina, S. V. *Biochim. Biophys. Acta* **1990**, *1020*, 25.
(8) Khangulov, S. V.; Barynin, V. V.; Voevodskaya, N. V.; Grebenko, A. I. *Biochim. Biophys. Acta* **1990**, *1020*, 305.
(9) Fronko, R. M.; Penner-Hahn, J. E.; Bender, C. J. *J. Am. Chem. Soc.* **1988**, *110*, 7554.
(10) Penner-Hahn, J. E. In *Manganese Redox Enzymes*; Pecoraro, V. L., Ed.; VCH: New York, 1992; pp 29–45.
(11) Waldo, G. S.; Fronko, R. M.; Penner-Hahn, J. E. *Biochemistry* **1991**, *30*, 10486.
(12) Debus, R. J. *Biochim. Biophys. Acta* **1992**, *1102*, 269.
(13) Vänngård, T.; Hansson, Ö.; Haddy, A. In *Manganese Redox Enzymes*; Pecoraro, V. L., Ed.; VCH: New York, 1992; pp 105–118.
(14) Hansson, Ö.; Wydrzynski, T. *Photosynth. Res.* **1990**, *23*, 131.
(15) Miller, A.-F.; Brudvig, G. W. *Biochim. Biophys. Acta* **1991**, *1056*, 1.
(16) Kono, Y.; Fridovich, I. *J. Biol. Chem.* **1983**, *258*, 13646.
(17) Zheng, M.; Dismukes, G. C. In *Research in Photosynthesis*; Murata, N., Ed.; Kluwer: Dordrecht, The Netherlands, 1992; Vol. II, pp 305–308.

0020-1669/94/1333-2677$04.50/0

was about 3.2 mg/mL. The 16-line EPR signal was present in the enzyme as isolated but was increased about 6-fold by treatment with NH_2OH and H_2O_2. For some experiments, the Mn(III)/Mn(IV) state was formed in the EPR tube by adding NH_2OH to 75 mM and then H_2O_2 to 7.5 mM just prior to freezing in liquid N_2 (sample 1). In later experiments, this state was produced by dialysis first against buffer A containing 20 mM NH_2OH and 50 mM H_2O_2, then against buffer A containing 50 mM H_2O_2, and finally against buffer A alone (sample 2). There was no apparent difference in the signal formed by the two methods, but the latter method improved signal stability and reproducibility.

X-band (9.2 GHz) EPR spectroscopy was performed using a Varian E-line spectrometer equipped with an E102 microwave bridge. P-band (15.5 GHz) EPR spectroscopy was performed using a homebuilt spectrometer described by Stevenson,[18] employing a Varian VA94 klystron tube as microwave source and a cylindrical cavity operating in the TE011 mode. The S-band (3.0 GHz) spectrometer was a homebuilt coaxial reflection system using an Englemann Model CC-24 solid-state tunable oscillator (about 70 mW), a Teledyne Model T-2563T-6 microwave circulator, a Miteq AMF-2B-2040-5 microwave preamplifier with a Sage Model DS300 Schottky diode detector, and a separate switchable bias arm with an ARRA adjustable phase shifter and attenuator. The tuned element was an aluminum loop-gap resonator[19] which accepted the same 5 mm outer diameter sample tubes as the X- and P-band spectrometers; this cavity contained a rhombic Fe(III) impurity evident as a signal at $g = 4.3$ (50 mT at 3.0 GHz). The loop-gap resonator was cooled together with the sample in the same home-made helium gas flow system as used for X- and P-band studies.

Data were digitized using a Tracor/Northern digital signal averager, Model NS570, interfaced to an IBM-compatible personal computer. Microwave frequency was monitored using a Hewlett Packard 5340A frequency counter, and magnetic field was calibrated with a Systron-Donner digital NMR gaussmeter, Model 3193.

The Fortran program used to simulate EPR spectra was based on perturbation theory, calculating the hyperfine coupling to third order as a perturbation of the Zeeman term. The spin Hamiltonian, $\mathcal{H} = \beta \mathbf{S}\cdot\mathbf{g}\cdot\mathbf{B} + \mathbf{S}\cdot\mathbf{A}\cdot\mathbf{I}$, was expressed in the Cartesian coordinate system with incident field B in the z direction such that

$$\mathcal{H} = \beta g \mathbf{S}_z\cdot\mathbf{B} + (A_x\mathbf{S}_x\cdot\mathbf{I}_x + A_y\mathbf{S}_y\cdot\mathbf{I}_y + A_z\mathbf{S}_z\cdot\mathbf{I}_z)$$

In the case of Mn catalase two hyperfine centers are involved and the perturbing hyperfine operator becomes

$$\mathcal{H}' = (A_{1x}\mathbf{S}_x\cdot\mathbf{I}_{1x} + A_{1y}\mathbf{S}_y\cdot\mathbf{I}_{1y} + A_{1z}\mathbf{S}_z\cdot\mathbf{I}_{1z}) + (A_{2x}\mathbf{S}_x\cdot\mathbf{I}_{2x} + A_{2y}\mathbf{S}_y\cdot\mathbf{I}_{2y} + A_{2z}\mathbf{S}_z\cdot\mathbf{I}_{2z})$$

The program calculated the matrix elements H_{ij}', where $H_{ij}' = \langle j|\mathcal{H}'|i\rangle$ and the zeroth-order wave function $|i\rangle = |m_s,m_{I1},m_{I2}\rangle$. The calculation was carried out for the case in which the hyperfine matrices were within the same principal-axis system as the $\mathbf{g}$ matrix. The energy, E_i, of each wave function $|i\rangle$ was found in terms of the microwave frequency from the zeroth- through third-order energies, E_{0i} through E_{3i}, given by perturbation theory.[20] This was done by numerically calculating each perturbation term, drawing from the elements of the matrix H_{ij}', rather than by deriving explicit expressions for the energies from the perturbation terms. Using the appropriate selection rule, $\Delta m_I = 0$, $\Delta m_s = \pm 1$, the transition energies, ΔE, were found in terms of microwave frequency. Then the field value for each transition was calculated from ΔE, which was set in accord with the experimental microwave frequency. When appropriately limited to second-order hyperfine terms and axial input matrices, this method of calculation was found to give simulated spectra essentially identical with those obtained by a method that employed the explicit expression for EPR transition energies derived by Bleaney[21] using second-order perturbation theory for axial systems.

For each simulated spectrum, the powder pattern was synthesized by calculating and summing spectra as the direction of the magnetic field was stepped over the sphere of the magnetic center. Gaussian line shapes were employed where W is the half-height line width of the absorption spectrum.

(18) Stevenson, R. C. Ph.D. Thesis, University of Michigan, 1982.
(19) Mehdizadeh, M.; Ishii, T. K.; Hyde, J. S.; Froncisz, W. *IEEE Trans. Microwave Theory Tech.* **1983**, *MTT-31*, 1059.
(20) Dalgarno, A. In *Quantum Theory*; Bates, D. R., Ed.; Academic Press: New York, 1961; Vol. I, pp 171–209.
(21) Bleaney, B. *Philos. Mag.* **1951**, *42*, 441.

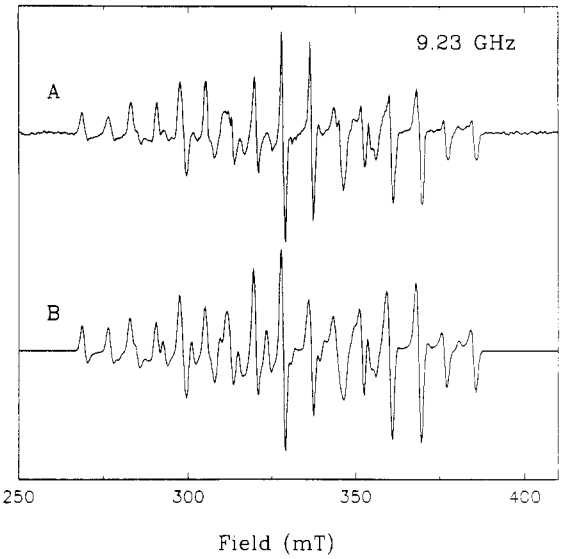

Figure 1. Experimental (A) and simulated (B) X-band (9.23 GHz) Mn(III)/Mn(IV) catalase EPR spectra. (A) Enzyme preparation and EPR spectroscopy were performed as described in the Experimental Section. EPR conditions include microwave power of 2 μW, modulation amplitude of 1.0 mT, and temperature of 9 K. (B) Spectral syntheses were carried out including third-order hyperfine terms as described in the text using the average EPR parameters $g_z = 1.9897$, $g_x = g_y = 2.0079$, $A_{1z} = 104.1 \times 10^{-4}$ cm^{-1}, $A_{1x} = A_{1y} = 141.6 \times 10^{-4}$ cm^{-1}, $A_{2z} = 83.5 \times 10^{-4}$ cm^{-1}, $A_{2x} = A_{2y} = 76.0 \times 10^{-4}$ cm^{-1}, $W_z = 1.14$ mT, and $W_x = W_y = 1.35$ mT.

Fits to the experimental spectra were obtained on a DEC VAX 8810 or 8600 microcomputer using the Levenberg–Marquadt nonlinear-least-squares minimization algorithm (MINPACK, Argonne National Laboratory). Averages of EPR parameters from the nine simulations were weighted according to the number of experimental spectra taken for each sample at a single frequency. The g values for one X-band spectrum (sample 2) were omitted from the average because of a small field shift error. The average parameters were used to synthesize the simulated spectra shown in the figures.

The vector projection model of spin coupling[22] was used to predict g factors and hyperfine constants expected for Mn(III)/Mn(IV) complexes on the basis of the values for selected Mn(III) and Mn(IV) monomers. For a system in which two spin vectors, S_1 and S_2, combine to form a total spin S, effective g factors and hyperfine constants for any principal axis may be estimated as

$$g^{\text{eff}} = g_1\frac{S_1\cdot S}{S^2} + g_2\frac{S_2\cdot S}{S^2}$$

$$A_i^{\text{eff}} = A_i\frac{S_i\cdot S}{S^2} \qquad i = 1, 2$$

where g_i and A_i are the g factor and hyperfine constant observed for the isolated spin S_i.

Results

The 16-line EPR signal from the Mn catalase of *L. plantarum* was examined at X-band (9.2 GHz), P-band (15.5 GHz), and S-band (3.0 GHz) microwave frequencies (Figures 1A, 2A and 3A, respectively). The number and intensity of lines in the EPR signal are consistent with its origin in an antiferromagnetically coupled Mn(III)/Mn(IV) dimer, as noted previously.[6-9,17] A more careful inspection of the X-band signal (Figure 1A) reveals several important features. Hyperfine anisotropy is apparent in the asymmetry of lines with respect to the baseline. The intensity pattern is not regular, and some of the lines are sharper than others (compare for example the lines at 328 and 345 mT). At P- and S-band (Figures 2A and 3A), the signal retains the same

(22) Sands, R. H.; Dunham, W. R. *Q. Rev. Biophys.* **1975**, *7*, 443.

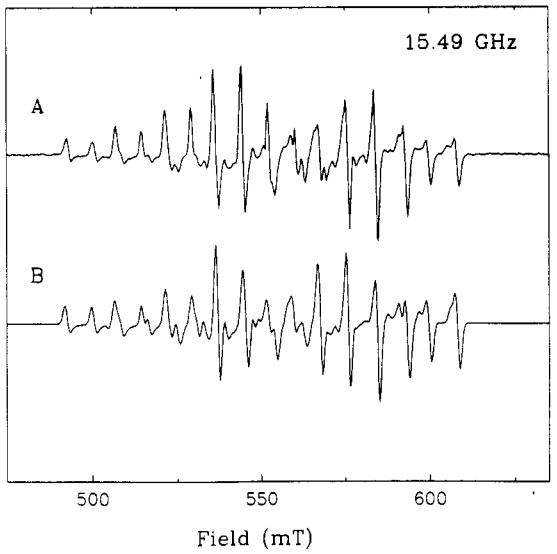

Figure 2. Experimental (A) and simulated (B) P-band (15.49 GHz) Mn(III)/Mn(IV) catalase EPR spectra. (A) Enzyme preparation and EPR spectroscopy were performed as described in the Experimental Section. EPR conditions include microwave power of 0.63 mW, modulation amplitude of 0.6 mT, and temperature of 10 K. (B) EPR simulation was carried out as described in the legend to Figure 1.

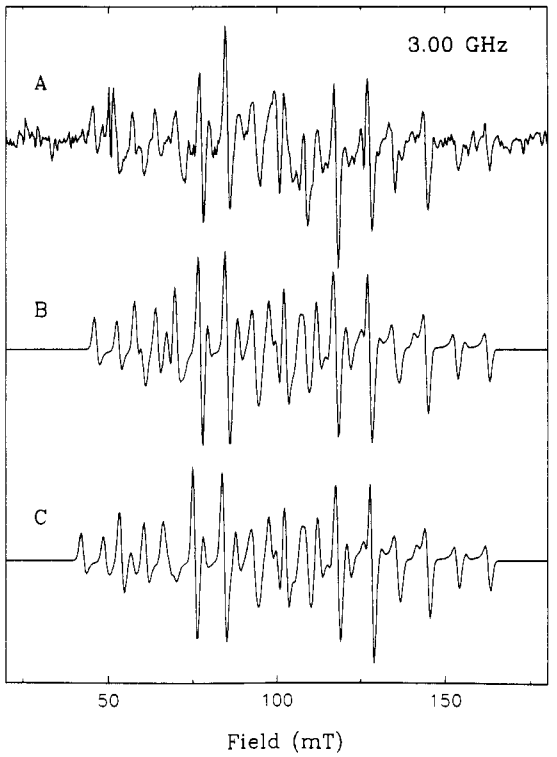

Figure 3. Experimental (A) and simulated (B, C) S-band (3.00 GHz) Mn(III)/Mn(IV) catalase EPR spectra. (A) Enzyme preparation and EPR spectroscopy were performed as described in the Experimental Section. EPR conditions include microwave power of 0.88 mW, modulation amplitude of 0.4 mT, and temperature of 50 K. A subtraction artifact appears at 49.9 mT ($g = 4.3$) in the S-band spectrum due to the subtraction of a rhombic Fe(III) signal from the cavity; this results in the apparent splitting of one of the low-field lines. (B, C) EPR simulations were carried out as described in the legend to Figure 1, including third-order hyperfine terms for spectrum B but limiting the hyperfine terms to second order for spectrum C.

general 16-line pattern; however, the relative intensities of many of the lines are altered.

EPR parameters were determined by nonlinear-least-squares minimization of each of nine experimental spectra, including one X- and four P-band spectra of sample 1 and one X- and three S-band spectra of sample 2. By use of a simulation routine written for $S = {}^1/_2$ systems, the ground state of Mn catalase was treated as an isolated doublet, thereby assuming a high negative coupling constant, J, between the two Mn ions.[23] This is expected, given the bis(μ-oxo)-bridged structure of Mn catalase[24] and is supported by the Curie law behavior of the signal up to at least 50 K.[25] Its validity is further confirmed by our ability to simulate the multifrequency spectra.

Table 1. EPR Parameters Found by Least-Squares Minimization for Experimental Mn Catalase Spectra from Three Frequencies

			hyperfine ($\times 10^4$ cm^{-1})				
PT order[a]	g_z	$g_x = g_y$	A_{1z}	$A_{1x} = A_{1y}$	A_{2z}	$A_{2x} = A_{2y}$	SD[b]
P-Band Spectra (15.49 GHz)[c]							
second order	1.9949	2.0096	104.36	141.37	83.80	75.17	31.52
third order	1.9949	2.0096	104.45	141.48	83.94	75.24	31.38
X-Band Spectra (9.23 GHz)[d]							
second order	1.9913	2.0066	103.33	141.38	83.24	75.98	62.61
third order	1.9911	2.0066	103.33	141.72	83.67	76.18	60.65
S-Band Spectra (3.00 GHz)[e]							
second order	1.9853	2.0110	103.09	136.35	77.34	73.64	714.8
third order	1.9831	2.0074	105.36	141.41	82.64	76.23	596.9
Average of Third-Order Fits[f]							
	1.9897	2.0079	104.11	141.58	83.48	75.96	

[a] The hyperfine values were calculated by extending the perturbation theory (PT) to either second or third order. [b] Standard deviations (SD) of the fits are relative to the scale of the experimental spectra, and so provide comparison between the second- and third-order fits at a single frequency only. [c] Average of four spectra from one sample. [d] Average of two spectra from two samples for hyperfine values; g factors from a single spectrum. [e] Average of three spectra from one sample. [f] X-band hyperfine values are doubly weighted to account for the use of two samples at that frequency.

The use of axial **g** and **A** matrices reproduced the features of the spectra well (Figures 1B, 2B, and 3B), while good fits could not be obtained using isotropic **g** or **A** matrices. Given the good fits obtained using axial matrices, minimizations using rhombic **g** and hyperfine matrices were not attempted. The weighted averages (± standard deviation) of the EPR parameters found by including the third-order perturbation terms were $g_z = 1.990 \pm 0.006$, $g_x = g_y = 2.008 \pm 0.002$, $A_{1z} = (104.1 \pm 0.9) \times 10^{-4}$ cm^{-1}, $A_{1x} = A_{1y} = (141.6 \pm 0.2) \times 10^{-4}$ cm^{-1}, $A_{2z} = (83.5 \pm 0.4) \times 10^{-4}$ cm^{-1}, and $A_{2x} = A_{2y} = (76.0 \pm 0.5) \times 10^{-4}$ cm^{-1} (Table 1). The refined spectral parameters were about the same at all three frequencies. These values are similar to those reported previously for simulation of X-band Mn(III)/Mn(IV) catalase spectra.[13,17]

In order to evaluate the importance of the third-order perturbation terms, fits were also carried out with the hyperfine calculation limited to the second-order perturbation expression (Table 1). For the X- and P-band data, the fitted parameters and the standard deviations of the fits were almost indistinguishable from those found using the third-order perturbation expression. The calculated hyperfine values were 0–0.51% lower at X-band and 0.08–0.16% lower at P-band than those found using third-order hyperfine terms, while g factors were the same as the third-order solutions except for a 0.01% deviation of one of the X-band values. At S-band, however, the second-order perturbation expression did not reproduce the experimental spectra as well as the third-order one, as reflected in the 20% improvement in the standard deviation of the fit using the third-order expression. Moreover, the fitted parameters found using only the second-order terms deviated substantially from those calculated in the other simulations, with hyperfine values 2.2–6.4% lower and g factors 0.1–0.2% higher than those found using third-order terms.

(23) The spin–spin interaction is here defined as $JS_1 \cdot S_2$.
(24) Waldo, G. S.; Yu, S.; Penner-Hahn, J. E. *J. Am. Chem. Soc.* **1992**, *114*, 5869.
(25) Waldo, G. S.; Penner-Hahn, J. E. Unpublished observations.

Table 2. *g* Factors and Hyperfine Constants for Experimental and Calculated Mn(III)/Mn(IV) Dimers

			hyperfine ($\times 10^4$ cm^{-1})			
			Mn(III) center		Mn(IV) center	
Mn species	g_z	$g_x = g_y$	A_{1z}	$A_{1x} = A_{1y}$	A_{2z}	$A_{2x} = A_{2y}$
Experimental Complexes						
Mn catalase[a]	1.990	2.008	104	142	83.5	76.0
$[Mn_2(\mu\text{-O})(TPP)_2X]$[b]		2.06		135		71
$[Mn_2(\mu\text{-O})_2(phen)_4]^{3+}$[c]		2.003		156		74
$[Mn_2(\mu\text{-O})_2(bpy)_4]^{3+}$[c]		2.003		156		74
$[Mn_2(\mu\text{-O})_2(\mu\text{-}O_2CMe)L_2]^{2+}$[d]		2.00		144		72
$[Mn_2(\mu\text{-O})(\mu\text{-}O_2CEt)_2(HB(pz)_3)_2]$[e]		2.0		148		72
$[Mn_2(\mu\text{-O})_2(\mu\text{-tren})_2]^{3+}$[f]	1.953	1.961	128	150		69
Calculated Hypothetical Complexes[g]						
Mn(III)/Mn(IV)[h]	1.986	2.006	106	165		70.8
Mn(III)/Mn(IV)[i]	1.989	2.013	106	165	75.0	71.1

[a] Values were found by fitting the experimental Mn(III)/Mn(IV) catalase spectra, as described in the text. [b] TPP = tetraphenylporphyrinate and X = OI(Br)Ph$^-$ or Br$^-$.[28] [c] phen = 1,10-phenathroline and bpy = 2,2′-bipyridyl.[29] [d] L = 1,4,7-triazacyclononane.[30] [e] pz = 1-pyrazolyl.[31] [f] tren = 2,2′,2″-triaminotriethylamine.[32] [g] Calculated for $S = {}^1/_2$ coupled dimers using the vector projection model of spin coupling, as described in the text. [h] Calculated on the basis of the following literature values: Mn(III) monomer in TiO_2 (tetragonal distortion of octahedral field) for which $g_z = 1.99$, $g_x = g_y = 2.00$, $A_z = 52.8 \times 10^{-4}$ cm^{-1}, and $A_x = A_y = 82.6 \times 10^{-4}$ cm^{-1};[35] Mn(IV) monomer in MgO (octahedral field) for which $g = 1.994$ and $A = 70.8 \times 10^{-4}$ cm^{-1}.[36,47] [i] Calculated on the basis of the values for the Mn(III) monomer in TiO_2 and the Mn(IV) monomer in SnO_2 (large rhombic distortion of octahedral field) for which $g_z = 1.991$, $g_x = g_y = 1.987$, $A_z = 75.0 \times 10^{-4}$ cm^{-1}, and $A_x = A_y = 71.1 \times 10^{-4}$ cm^{-1} (average of 72.2×10^{-4} and 70.0×10^{-4} cm^{-1}).[36]

Examination of the third-order expression shows that it corrects line position with a shift that is generally inward. Comparison of simulations limiting the hyperfine expression to second versus third order but using the same parameters (Figures 3C and 3B) shows that, without the third-order terms, lines at the low-field end of the S-band spectrum are visibly misaligned and too far downfield.

The assumption that the Mn catalase **g** and hyperfine matrices were in the same principal-axis system is supported by approximate agreement between the hyperfine anisotropies of the Mn catalase and those calculated for hypothetical Mn(III)/Mn(IV) complexes in Table 2 (see Discussion for further comparison). Significant deviation of a true hyperfine principal-axis system from the assumed axis system would result in apparent A_x, A_y, and A_z values that are linear combinations of the true principal-axis values. This would have the effect of decreasing the observed anisotropy of the Mn catalase hyperfine matrix. Because the experimental hyperfine anisotropies were fairly pronounced relative to the anisotropies calculated for the hypothetical Mn(III)/Mn(IV) centers, particularly for the Mn(IV) center, the assumption of a single principal-axis system is reasonable. Any small errors that might have resulted from this assumption cannot be known without carrying out single-crystal EPR studies of the spin center. The successful use of a single principal-axis system is consistent with an orbital configuration that is symmetrical between the two Mn ions.

Several additional factors could, in principle, affect the experimental spectra but were not included in the simulations because their effects were minor. These include cross terms between nuclei, "forbidden transitions", and nuclear electric quadrupole effects. Internuclear cross terms result from an electron-mediated interaction between nuclei. These terms, if included, would come in as part of the second-order hyperfine correction and hence become more pronounced at lower frequencies. The cross terms are zero for isotropic nuclei and increase in magnitude with increasing anisotropy. Their magnitude can be estimated from the EPR parameters found here for Mn catalase using a formula given by Weil.[26] The largest shifts would be only 0.3×10^{-4} cm^{-1} at 9.2 GHz and 1×10^{-4} cm^{-1} at 3.0 GHz for the outermost lines. The shifts would decrease upon going inward since the size of the cross term for each transition is proportional to $m_{I1}m_{I2}$. The second-order cross terms are thus an order of magnitude smaller than the third-order hyperfine term and will not make an important contribution.

The "forbidden transitions" are those for which $\Delta m_I \neq 0$. Since there were no obvious transitions in the spectra that were not accounted for in the simulation, omission of forbidden transitions does not appear to have caused any problems in fitting accuracy. Forbidden transitions have most commonly been observed for high-spin monomeric centers with low symmetry, such as monoclinic or triclinic.[27] The lack of forbidden transitions in this case is not surprising since the signal arises from an $S = {}^1/_2$ ground state, although it is composed of two high-spin ions. In addition, the Mn(III)/Mn(IV) catalase system probably has relatively high symmetry, as suggested by the apparent coincidence of the principal-axis systems for **g** and hyperfine matrices. The nuclear electric quadrupole term was also not included in the calculation. Although it is nonzero for these $I = {}^5/_2$ nuclei, it is expected to be negligible. The accuracy of the fits using the same parameters at all three frequencies again indicates that this assumption is good.

No change in line width was observed with changing microwave frequency, indicating that *g*-strain broadening was not important for the Mn catalase EPR signal. Thus the microdistribution of conformations of the spin center did not determine the line width. Minimization of the Gaussian line widths gave $W_z = 1.1 \pm 0.1$ mT and $W_x = W_y = 1.4 \pm 0.1$ mT. These line widths are significantly narrower than those seen for synthetic Mn(III)/Mn(IV) complexes that have been studied by EPR.[28-32] The lack of a frequency-dependent broadening effect for this biological Mn center is noteworthy, given the prevalence of *g*-strain broadening in numerous biological Fe and Cu centers,[33] and is presumably due to the smaller anisotropies of the Mn(III) and Mn(IV) **g** matrices.

Discussion

Chemical Evaluation. The EPR parameters determined for the Mn(III)/Mn(IV) catalase are compared with the literature values for several synthetic Mn(III)/Mn(IV) dimers in Table 2. On the basis of the 2.67-Å Mn–Mn distance determined by EXAFS, Mn(III)/Mn(IV) catalase is believed to contain two μ-oxo bridging ligands and perhaps an additional μ-carboxylato bridge.[24] Thus $[Mn_2(\mu\text{-O})_2(O_2CMe)L_2]^{2+}$ may be the complex that is most similar in structure to the Mn(III)/Mn(IV) catalase. In general, the spectra of the synthetic dimers are similar to that of Mn catalase. Each has 16 main hyperfine lines centered at $g = 2.0$ with $A_1 = (140\text{–}150) \times 10^{-4}$ cm^{-1} for the Mn(III) center and $A_2 = (70\text{–}80) \times 10^{-4}$ cm^{-1} for the Mn(IV) center. Like the Mn catalase spectra the EPR spectra for $[Mn_2(\mu\text{-O})_2(\mu\text{-tren})_2]^{3+}$, $[Mn_2(\mu\text{-O})_2(TPP)_2X]$, $[Mn_2(\mu\text{-O})_2(phen)_4]^{3+}$, and $[Mn_2(\mu$-

(26) Weil, J. A. *J. Magn. Reson.* **1975**, *18*, 113.
(27) Misra, S. K.; Upreti, G. C. In *Electronic Magnetic Resonance of the Solid State*; Weil, J. A., Ed.; The Canadian Society for Chemistry: Ottawa, Canada, 1987; pp 69–81.
(28) Dismukes, G. C.; Sheats, J. E.; Smegal, J. A. *J. Am. Chem. Soc.* **1987**, *109*, 7202.
(29) Cooper, S. R.; Dismukes, G. C.; Klein, M. P.; Calvin, M. *J. Am. Chem. Soc.* **1978**, *100*, 7248.
(30) Wieghardt, K.; Bossek, U.; Zsolnai, L.; Huttner, G.; Blondin, G.; Girerd, J.-J.; Babonneau, F. *J. Chem. Soc., Chem. Commun.* **1987**, 651.
(31) Sheats, J. E.; Czernuszewicz, R. S.; Dismukes, G. C.; Rheingold, A. L.; Petrouleas, V.; Stubbe, J.; Armstrong, W. H.; Beer, R. H.; Lippard, S. J. *J. Am. Chem. Soc.* **1987**, *109*, 1435.
(32) Hagen, K. S.; Armstrong, W. H.; Hope, H. *Inorg. Chem.* **1988**, *27*, 967.
(33) Hagen, W. R. *J. Magn. Reson.* **1981**, *44*, 447.

$O)_2(O_2CMe)L_2]^{2+}$ all show considerable anisotropy.[34] A_{1x} for Mn catalase is lower than A_1 for most of the synthetic dimers, with $[Mn_2(\mu\text{-}O)_2(TPP)_2X]$ and $[Mn_2(\mu\text{-}O)_2(O_2CMe)L_2]^{2+}$ giving the best comparison. However, A_{2x}, A_{2y}, and A_{2z} for Mn catalase are higher than A_2 found for any of the synthetic complexes, suggesting a slightly less covalent Mn(IV) center or a lower ligand field energy in Mn catalase.

The hyperfine constants and g factors obtained from the simulated spectra are also compared with those predicted from the vector projection model of spin coupling (Table 2). The environment of the Mn(III) center can be compared with that of Mn(III) in TiO_2,[35] one of the few known examples of a d^4 configuration studied by EPR. The environment of this Jahn–Teller ion becomes tetragonally distorted, producing an excited state that is energetically close to the ground state. Orbital inequivalence thus results in g and hyperfine anisotropy. Since the Mn(III) ion in catalase is probably coordinated to six N/O-type ligands[24] and since A_x, $A_y > A_z$ both for the catalase Mn(III) and for Mn(III) in TiO_2, the comparison is reasonable. However, the hyperfine anisotropy of the catalase Mn(III) is not as great as expected on the basis of the calculation using Mn(III) in TiO_2. This may suggest a lower degree of distortion of the Mn(III) center in Mn catalase. On the other hand, the overall magnitude of the hyperfine coupling both in Mn catalase and in the synthetic dimers is lower than predicted by Mn(III) in TiO_2, which is likely to be a reflection of different types of ligands. Thus Mn(III) in Mn catalase may be bonded to ligands that are more covalent than those in TiO_2 or to stronger field ligands which participate in a greater degree of back-bonding.

A small degree of hyperfine anisotropy was also found for the Mn(IV) center of Mn catalase. Monomeric Mn(IV) usually shows little or no g or hyperfine anisotropy because in an octahedral field this d^3 ion is an orbital singlet with excited states lying at energies that are large compared with the spin–orbit coupling energy. In Mn catalase, the Mn(IV) center shows $A_z > A_x$, A_y by 7.5×10^{-4} cm^{-1}. This is greater by about 4×10^{-4} cm^{-1} than even that for Mn(IV) in SnO_2,[36] which has a large rhombic distortion from octahedral symmetry. In addition, the Mn(IV) center in Mn(III)/Mn(IV) catalase shows higher hyperfine values overall, which may result from lower covalency with ligands than in SnO_2 or MgO. These differences suggest that the nature of the Mn(IV) ion in the dimer is significantly different from that of monomeric Mn(IV), perhaps because of a lower ligand field energy or an increased spin–orbit coupling energy. It is likely that the differences are related to the presence of the μ-oxo bridge between Mn ions.

Simulation Method and the OEC Signal. Simulation of the S_2 multiline signal from the OEC represents an important problem in EPR spectral computation. Although under study for over a decade, the complex hyperfine structure has not been unambiguously accounted for. Structural and chemical similarities have been demonstrated for the Mn(III)/Mn(IV) catalase and the S_2 O_2-evolving complex; both contain high-oxidation-state Mn, and the EXAFS of each indicates the presence of μ-oxo-bridged Mn dimer(s).[12-14,24] Similarities in the EPR signals further support the comparison between them, although the OEC signal arises from as many as four coupled Mn ions. The significant g and hyperfine anisotropy found for the Mn catalase signal demonstrates the influence of the d^4 Mn(III) ion. The $g = 2$ multiline signal from the OEC is also believed to arise from a Mn(III)-containing cluster, which would be consistent with the hyperfine anisotropy observed in oriented photosystem II-enriched membranes.[37,38]

Attempts to simulate the OEC signal published thus far have been carried out using perturbation theory to calculate the hyperfine shifts but limiting this term to second order. Early studies of the X-band signal compare it to the signals expected for various coupled Mn(III)- and Mn(IV)-containing dimers[39-41] and tetramers,[42-44] employing isotropic hyperfine matrices and usually isotropic g factors. A recent simulation based on a Mn tetramer model showed substantial improvement over prior simulation attempts.[45] In this study, which again assumed isotropic **g** and hyperfine matrices, a minimization routine was employed to arrive at two possible empirical solutions. However, many details such as structure within the main lines and poorly resolved outer lines remain to be incorporated. In another recent study simulations based on 3Mn(III)/Mn(IV) and Mn(III)/3Mn(IV) tetramer models also reproduced the main characteristics of the multiline signal fairly well.[17] In this case, an axial hyperfine expression was employed, although the simulation method was not fully described. Together these simulations represent four possible different solutions to the OEC multiline signal, leaving much ambiguity in making a reliable interpretation.

We believe that an accurate and unambiguous solution to the OEC multiline signal rests on an approach that combines two aspects: computational limitations must be overcome and data from more than one frequency must be included. Since the OEC multiline signal includes hyperfine anisotropy[37,38] and probably g anisotropy as well, on the basis of the generally accepted presence of one or more Mn(III) ions, a complete simulation of the signal must include anisotropic terms. A serious limitation of previous computation methods based on perturbation theory is that the hyperfine calculation has not been extended beyond a second-order axial expression derived by Bleaney.[21] Furthermore, multifrequency data for the OEC multiline signal have been obtained, including Q-band (35 GHz)[46] and S-band (3.9 GHz),[37] with the S-band signal revealing the complexity of the hyperfine structure most clearly. However, as stated in the present work, perturbation theory limited to second order will not be sufficient at such a low frequency. Computation must include higher order perturbation terms or use the matrix diagonalization approach.

The simulation method employed here for the Mn catalase signal is capable of calculating rhombic spectra using perturbation theory to third order and can be further extended to higher order perturbation terms. It avoids the time-consuming computation involved in a matrix diagonalization approach. This consideration becomes particularly important when two or more high-spin nuclei are involved. For Mn catalase, the effective $S = {}^1/_2$ system coupled to two $I = {}^5/_2$ nuclei results in 72 energy levels. Diagonalization of a 72×72 matrix takes about 300 times more CPU time than the equivalent calculation by the perturbation method. This time difference would become overwhelming if four Mn nuclei were included. Although matrix diagonalization will ultimately

(34) The spectra for $[Mn_2(\mu\text{-}O)_2(TPP)_2X]$, $[Mn_2(\mu\text{-}O)_2(phen)_4]^{3+}$, and $[Mn_2(\mu\text{-}O)_2(O_2CMe)L_2]^{2+}$ were analyzed using an isotropic spin Hamiltonian; however, anisotropy is visible in each spectrum.

(35) Gerritsen, H. J.; Sabisky, E. S. *Phys. Rev.* **1963**, *132*, 1507.
(36) McGarvey, B. R. In *Transition Metal Complexes*; Carlin, R. L., Ed.; Marcel Dekker: New York, 1966; Vol. 3, pp 89–201.
(37) Haddy, A.; Aasa, R.; Andréasson, L.-E. *Biochemistry* **1989**, *28*, 6954.
(38) Rutherford, A. W. *Biochim. Biophys. Acta* **1985**, *807*, 189.
(39) Dismukes, G. C.; Siderer, Y. *Proc. Natl. Acad. Sci. U.S.A.* **1981**, *78*, 274.
(40) Hansson, Ö.; Andréasson, L.-E. *Biochim. Biophys. Acta* **1982**, *679*, 261.
(41) Hansson, Ö.; Andréasson, L.-E.; Vänngård, T. In *Advances in Photosynthesis Research*; Sybesma, C., Ed.; Martinus Nijhoff: The Hague, 1984; Vol. I, pp I.3.307–I.3.310.
(42) Dismukes, G. C.; Ferris, K.; Watnick, P. *Photobiochem. Photobiophys.* **1982**, *3*, 243.
(43) de Paula, J. C.; Beck, W. F.; Brudvig, G. W. *J. Am. Chem. Soc.* **1986**, *108*, 4002.
(44) de Paula, J. C.; Beck, W. F.; Miller, A.-F.; Wilson, R. B.; Brudvig, G. W. *J. Chem. Soc., Faraday Trans. 1* **1987**, *83*, 3635.
(45) Bonvoisin, J.; Blondin, G.; Girerd, J.-J.; Zimmermann, J.-L. *Biophys. J.* **1992**, *61*, 1076.
(46) Hansson, Ö.; Aasa, R.; Vänngård, T. *Biophys. J.* **1987**, *51*, 825.
(47) Abragam, A.; Bleaney, B. *Electron Paramagnetic Resonance of Transition Ions*; Dover: New York, 1970.

give the most accurate results, the present work demonstrates that the third-order perturbation expression is adequate for simulating multifrequency EPR spectra from biological binuclear Mn centers. The Mn catalase spectra serve as an excellent test case for more complex problems such as the OEC multiline EPR signal.

Acknowledgment. This work was supported by grants from the National Institutes of Health (GM-45205 to J.P.-H. and GM-32785 to R.H.S.) and the Office of the Vice President for Research, University of Michigan, to R.H.S. A.H. was supported in part by fellowships from the Program in Protein Structure and Design, University of Michigan, and the Mayo Foundation. We thank J. A. Weil for advice regarding internuclear cross terms and for use of a matrix diagonalization program developed by him and co-workers. We also thank W. R. Dunham and E. H. Hellen for many helpful discussions.